CHAPTER II
LITERATURE REVIEW

Jet fuel is a type of aviation fuel designed for use in aircraft powered by gas turbine engines. The most commonly used fuels for commercial aviation are Jet A and Jet A-1, Jet A and Jet A-1 are kerosene type fuels. The primary difference is the lower freezing point of A-1: Jet A's is −40 °C and Jet A-1's is −47 °C. Jet B is another grade of jet fuel used in very cold climate which is a blend of gasoline and kerosene.

Jet fuel is a mixture of a large number of different hydrocarbons, possibly as many as a thousand or more. The range of their sizes (molecular weights or carbon numbers) is restricted by the requirements for the product, for example, freezing point or smoke point. Kerosene-type jet fuels (including Jet A and Jet A-1) have a carbon number distribution between about 8 and 16 carbon numbers; wide-cut or naphtha-type jet fuel (including Jet B), between about 5 and 15 carbon numbers.

2.1 Renewable Diesel

Renewable diesel can be produced via hydrotreating which is another route to produce of renewable diesel or renewable liquid alkane substitute from vegetable oils and fats, which contain the triglyceride, as shown in Figure 2.1. The standard hydrotreating conditions are 300 – 450 °C with conventional hydrotreating catalysts (i.e. NiMo/γ-Al_2O_3, sulfided NiMo/γ-Al_2O_3, Pd/C). In hydrotreating process, the hydrocarbons are produced by the three difference pathways: (i) hydrodeoxygenation (or dehydration/hydrogenation), (ii) hydrodecarboxylation, and (iii) hydrodecarbonylation. In hydrodeoxygenation reaction, the hydrocarbon chain is broken, and undesired oxygen is removed, leading to a production of straight-chain hydrocarbons suitable for diesel fuel. The normal alkanes originating from HDO have the same carbon number as the original fatty acid chain, i.e. even carbon number, typically 16 or 18.

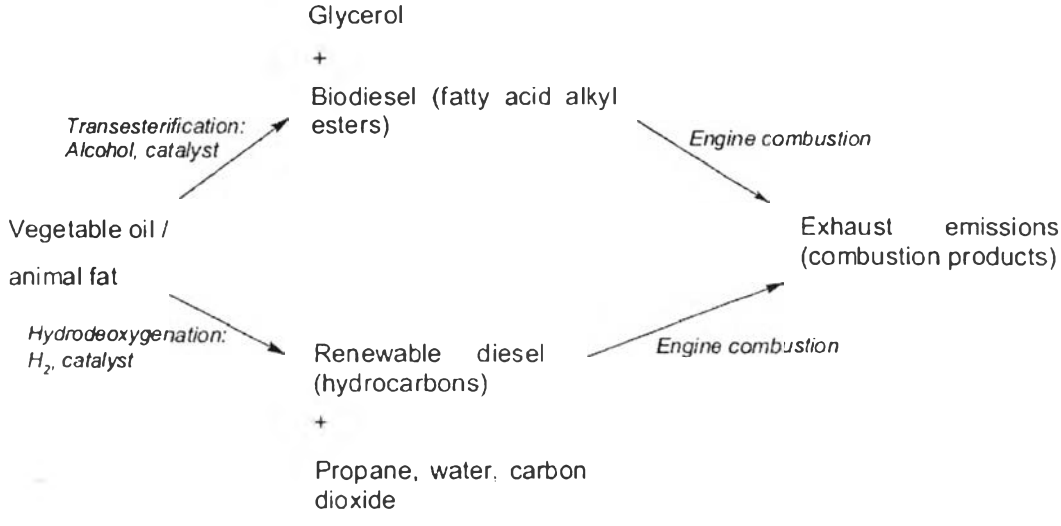

Figure 2.1 Flowchart for transformation of lipid materials (biodiesel and renewable diesel by hydrodeoxygenation) to products of engine combustion (Knothe, 2010).

Renewable liquid alkanes or renewable diesel can be produced by hydrotreating of vegetable oils at standard hydrotreating conditions (i.e. 300 – 450 °C) with conventional hydrotreating catalysts (sulfided NiMo/Al_2O_3, NiMo/γ-Al_2O_3). Huber *et al.* (2007) studied hydrotreating of pure sunflower oil in a fixed bed reactor with a sulfided NiMo/γ-Al_2O_3 catalyst. The reaction was done at temperature ranging from 300 to 450 °C, pressure of 50 bar, LHSV 4.97 h^{-1} and H_2 to feed ratio of 1600 ml H_2/ml liquid feed. The products obtained were analyzed by GC. It was found that the fraction distilled from 250 to 350 °C was the major distillation fraction. This fraction is mostly n-C15, n-C16, n-C17, and n-C18. The mixture in this fraction occurred at reaction temperature of 350 °C. The reaction pathways involves hydrogenation of the C=C bonds of the vegetable oils followed by alkane production by three different pathways: decarbonylation, decarboxylation and hydrodeoxygenation as shown in Figure 2.2. Moreover, the straight chain alkanes can undergo isomerization and cracking to produce lighter and isomerized alkanes. In addition, they proposed that the catalyst and reaction condition play an important role to determine the yield of the decarbonylation, decarboxylation and hydrodeoxygenation pathways.

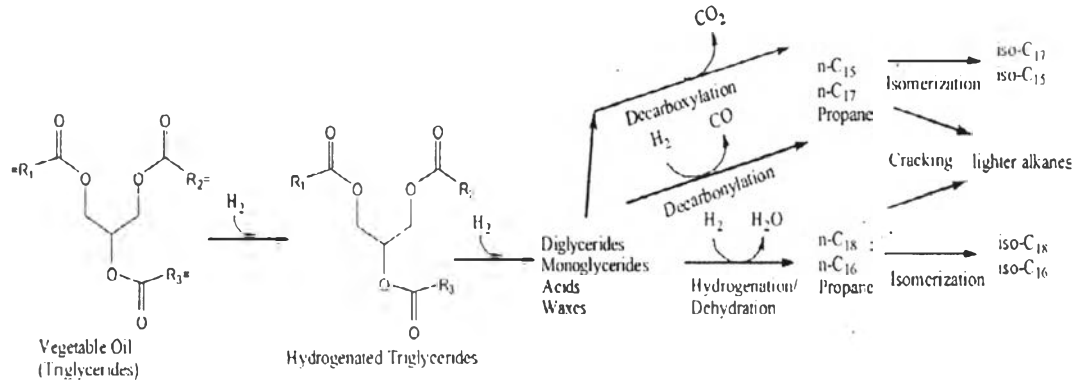

Figure 2.2 The reaction pathway for conversion of triglycerides to renewable diesel (Huber *et al.*, 2007).

In the first step of this reaction pathway the triglyceride is hydrogenated and broken down into various intermediates which are monoglycerides, diglycerides and carboxylic acids. These intermediates are then converted into alkanes by three different pathways: decarboxylation, decarbonylation and hydrodexogenation (or dehydration/hydrogenation). Moreover, the straight chain alkanes can undergo isomerization and cracking to produce lighter and isomerized alkanes. In addition, they proposed that the catalyst and reaction conditions play an important role to determine the yield of the decarbonylation, decarboxylation and hydrodeoxygenation pathways.

There are several possible reaction pathways for a production of straight-chain hydrocarbons, shown as Figure 2.3. Carboxylic acids have used to represent feedstock and similar equations can be written for alkane production from mono-, di- or tri-glycerides. Fatty acids can be directly decarboxylated or decarbonylated. Direct decarboxylation removes the undesired oxygen by releasing carbon dioxide and producing aliphatic hydrocarbon chains with one carbon atom less than in the original feed, while direct decarbonylation removes the undesired oxygen by forming carbon monoxide and water, as explained by reactions I and II. Moreover, the fatty acid can be deoxygenated by adding hydrogen leading to a production of straight-chain hydrocarbons and undesired oxygen will be removed through formation of water, as explained by reactions III (Snare *et al.*, 2006). This pathway involves

bifunctional catalysis that contains sites for hydrogenation reactions (possibly NiMo sites) and for dehydration reactions (acid catalytic sites). It is possible that the free fatty acid intermediates are catalyzing the dehydration reaction. The hydrogen requirements decreases as hydrodeoxygenation > decarbonylation pathway > decarboxylation pathway. (Huber *et al.*, 2007)

Liquid phase reactions

						ΔG_{573} (kJ/mol)	ΔH_{573} (kJ/mol)
I.	Decarboxylation:	R-COOH	⟶	R-H	+ CO_2 (g)	-83.5	9.2
II.	Decarbonylation:	R-COOH	⟶	R'-H	+ CO (g) + H_2O (g)	-17.0	179.1
III.		R-COOH + H_2 (g)	⟶	R-H	+ CO (g) + H_2O (g)	-67.6	48.1
IV.	Hydrogenation:	R-COOH + $3H_2$ (g)	⟶	$R-CH_3$	+ $2H_2O$ (g)	-86.1	-115.0

R = saturated alkyl group *R' = unsaturated alkyl group*

Figure 2.3 The possible liquid-phase reaction pathways for production of straight-chain hydrocarbons from fatty acids. (Snare *et al.*, 2006)

In addition to the liquid-phase reactions, the water gas shift and methanation reaction are occurred with a number of carbon monoxide, carbon dioxide, hydrogen, and water formed during decarbonylation/decarboxylation reaction. The water-gas-shift reaction may balance the concentrations of CO and CO_2, while methanation reaction of fatty acids gives methane and water, shown as Figure 2.4.

Gas phase reactions

								ΔG_{573} (kJ/mol)	ΔH_{573} (kJ/mol)
V.	Methanation:	CO_2	+	$4H_2$	⇌	CH_4	+ $2H_2O$	-61.2	-177.2
VI.	Methanation:	CO	+	$3H_2$	⇌	CH_4	+ H_2O	-78.8	-216.4
VII.	Water-gas-shift	CO	+	H_2O	⇌	H_2	+ CO_2	-17.6	-39.2

Figure 2.4 Gas phase reactions of CO or CO_2 with H_2 or H_2O. (Snare *et al.*,2006)

Jindarat studied deoxygenation of beef fat for the production of hydrogenated biodiesel over Pd supported mesoporous titania catalysts. The effect of catalyst preparation was studies. Hydrogenated biodiesel is one of the biofuels that has gained attention in recent years due to its superior fuel properties compared to conventional biodiesel. In our previous work, Pd supported TiO_2 was shown to be a promising catalyst for the deoxygenation of triglycerides towards hydrogenated biodiesel. In this research, the effect of catalyst preparation on the production of hydrogenated biodiesel was evaluated. Pd/TiO_2 catalysts were prepared by incipient wetness impregnation (IWI) and photochemical deposition (PCD) by using both mesoporous TiO_2 supports synthesized via a combined sol-gel process with a surfactant-assisted templating method (SG-TiO_2) and commercial TiO_2 support (P25-TiO_2). Moreover, Pd/TiO_2 catalyst synthesized via a combined single-step sol-gel process (SSSG) with surfactant-assisted templating method was conducted to compare with two other methods. The catalysts were tested in a fixed-bed continuous flow reactor at 500 psig, 325 °C, H_2/feed molar ratio of 30, and liquid hourly space velocity (LHSV) of 4 h^{-1}. The products obtained from all catalysts were in the specification range of diesel fuel and the main diesel products were n-heptadecane and n-pentadecane resulting from decarboxylation/decarbonylation pathway. Among all catalysts, SSSG Pd/TiO_2 catalyst provided the highest conversion of triglycerides and selectivity of the desired products. The high activity and product selectivity of SSSG could be due to its high surface area and dispersion of Pd.

2.2 Hydrotreated Renewable Jet Fuel

Hydrotreated renewable jet fuel is a renewable fuel that can be used instead of jet fuel derived from petroleum but Hydrotreated renewable jet fuel is produced from biomass such as algae, jatropha and palm oil. Hydrotreated renewable jet fuel usually blends with petroleum-based Jet A/Jet A-1 fuel and 50 percent sustainable biofuels.

Jongpatiwut *et al.* (2013) studied catalyst development for the production of hydrotreated renewable jet (HRJ) fuel from hydrogenated biodiesel in commercial scale. The production of hydrotreated renewable jet fuel from hydrogenated biodiesel

was investigated over Pt supported HY catalysts with various metal loadings (0.05, 0.1, 0.3, 0.5, 0.7, and 0.9 wt %) and tested in a continuous flow packed-bed reactor at 310 °C, 500 psig, liquid hourly space velocity (LHSV) of 1 h^{-1}, and H_2/feed molar ratio of 30. The main products obtained over 0.1Pt/HY, 0.3Pt/HY, 0.5Pt/HY, 0.7Pt/HY and 0.9Pt/HY were in jet fuel boiling point range ($C_9 - C_{14}$) but the main product of 0.05Pt/HY was in gasoline boiling point range ($C_5 - C_8$) due to its high acidity. The Pt supported HY catalysts (0.1Pt/HY, 0.3Pt/HY, 0.5Pt/HY, 0.7Pt/HY and 0.9Pt/HY) resulted in a high conversion and high yield in jet fuel boiling range with higher isomerized paraffins in diesel fuel boiling range. Especially, products were obtained from 0.3Pt/HY, giving jet yield of 35.19 wt% while 0.1Pt/HY gave jet yield of 29.63 wt%. Then, we selected 0.1Pt/HY to study stability, and effect of H_2/feed molar ratio because 0.1Pt/HY can reduce Pt contents about three times from 0.3Pt/HY. Moreover, the optimum reaction condition was found at 310 °C, 500 psig, LHSV of 1 h^{-1}, and H_2/feed ratio 30.

The effect of catalyst preparation methods over the Pt/HY catalyst on the hydrocracking and hydroisomerization of hydrogenated biodiesel for the production of hydrotreated renewable jet fuel was investigated. The different preparation methods gave the different conversions and product selectivity. There were three main groups of liquid products which were gasoline boiling point range ($C_5 - C_8$), jet fuel boiling point range ($C_9 - C_{14}$), and isomerized paraffins in diesel fuel boiling range ($C_{15} - C_{18}$). Among Pt supported HY catalysts, Pt/HY catalyst synthesized via ion-exchange (IE) gave the highest conversion of hydrogenated biodiesel and hydrotreated renewable jet fuel yield that cause by the high dispersion of Pt on HY support of IE catalyst among other Pt/HY. Besides, the high catalytic activity and the high desired product selectivity also corresponded to the low amount of hard coke deposition on the catalyst.

2.3 Raw Materials in Hydrotreated Renewable Jet Production

Vegetable oils are used as raw materials of hydrotreated renewable jet fuel production because it is one type of the renewable fuels. Vegetable oils have become more attractive recently because of its environmental benefits and the fact that it is

made from renewable resources. The examples of vegetable oils used in hydrotreated renewable jet fuel and biodiesel production are devised to edible oils and non-edible oils. In the past, the researchers used edible oils such as palm oil, rapeseed oil, sunflower oil, soybean oil, etc. which become a major source of hydroteated renewable jet production but when edible oils were used as a feedstock, the food chain problems occurred. Then, the researchers changed edible oils to non-edible oils such as Jatropha curcas (Jatropha), Pongamina pinnata (Karanja), Madhua indica, Calophylluminophyllum (Polanga), Hevea brasiliensis (Rubber), etc. Jatropha is a plant that produces seeds containing inedible lipid oil that can be used to produce fuel. Each seed produces 30 to 40 % of its mass in oil. Jatropha can be grown in a range of difficult soil conditions, including arid and otherwise non-arable areas, leaving prime land available for food crops. The seeds are toxic to both humans and animals and are therefore not a food source.

Vegetable oils and fats are lipid materials derived from plants. Physical properties of oils are liquid at room temperature, and fats are solid. Chemically, both fats and oils are composed of triglycerides, as contrasted with waxes which lack glycerin in their structure. The molecule of triglyceride is composed of three long chain fatty acids of 8 to 22 carbons attached to a glycerol backbone (Juan J.C. *et al.*, 2011).

2.4 Core-shell Catalyst

Okada *et al.*, (2012) reported the importance of the structural design of heterogeneous catalysts for one-pot reaction. The most popular catalysts for the one-pot reaction are Pd nanoparticles (NPs) supported on titanium silicate-1 (Pd/TS-1) or Pd NPs supported on Ti-containing mesoporous silica (Pd/Ti-MS). Unfortunately, the intermediate H_2O_2 is easily decomposed by the Pd catalyst, thereby competing against its synthesis, because the random location of both active sites accelerate the dispersion and decomposition of H_2O_2 prior to contact with the Ti site, which results in low utilization efficiency of diluted H_2O_2 as shown in Figure 2.5 (a). Therefore, a series of core–shell catalysts consisted of SiO_2 core, Pd nanoparticles (NPs), and Ti containing mesoporous silica (Ti-MS) shell with precise control of the Pd NPs

positions were synthesized as depicted in Figure 2.5 (b), the mesopore diameter, and the thickness of the Ti-MS shell. The catalytic potentials were evaluated for one-pot oxidation reactions involving the direct synthesis of hydrogen peroxide (H_2O_2) from H_2 and O_2 gases by the Pd NPs and the subsequent oxidation reaction of sulfide by the isolated Ti^{IV} species using in situ produced H_2O_2 in the mesoporous silica. The precise architecture of the core–shell catalyst significantly enhanced the catalytic performance by a factor of 20, and the catalyst exhibited excellent activity and selectivity toward sulfoxide as compared to the commonly employed Pd-supported/Ti-zeolite (Pd/TS-1) catalyst. This result provides a new perspective of heterogeneous catalysts aimed at developing environmentally friendly chemical processes.

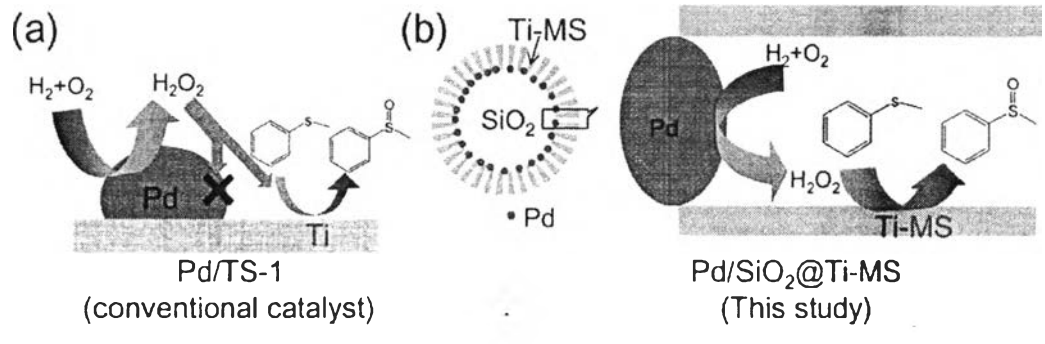

Figure 2.5 Schematic illustration of the one-pot oxidation reaction using (a) Pd/TS-1 and (b) the Pd/SiO_2@Ti-MS core–shell catalyst (Okada *et al.*, 2012).

2.4.1 Effect of the Pd NPs Location in the Core–shell Catalyst

Pd/SiO_2@Ti-MS was synthesized as follows. The $PdCl_2$ precursor was first deposited on the surface of spherical SiO_2 NPs (280 nm average diameter), followed by reduction in the presence of sodium formate. After formation of the Pd NPs, further coating with the Ti-MS shell was performed using cetyltrimethylammonium bromide (CTAB) as a structure-directing agent (SDA), tetraethyl orthosilicate (TEOS) as a silica source, and tetrapropyl orthotitanate (TPOT) as a Ti source. To clarify the effect of the core–shell structure on the catalytic properties, it is not appropriate to compare the core–shell catalyst with a

conventional catalyst (e.g., Pd/TS-1), because the environments around the Ti sites are quite different. Therefore, two reference samples, SiO_2@Pd(R)/Ti-MS and SiO_2@Pd(S)/Ti-MS, were synthesized as conventional model catalysts. In the case of SiO_2@Pd(R)/Ti-MS, where (R) denotes random, the Pd NPs were deposited after calcination, which allowed random distribution of Pd NPs within the mesoporous shell structure. SiO_2@Pd(S)/Ti-MS, where (S) denotes surface, was obtained by first coating the SiO_2 core with the Ti-MS shell, followed by loading of the Pd NPs. High resolution-transmission electron microscopy (HRTEM) images of Pd/SiO_2@Ti-MS and the two model catalysts are presented in Figure 2.6. All samples had spherical NPs with nonporous SiO_2 cores, Ti-MS shells with channels oriented perpendicular to the core surface, and Pd NPs. The Pd NPs were present at the intended sites: the boundary between the SiO_2 core and the mesoporous silica shell, randomly distributed within the mesopores of the silica shell, and on the surface of the mesoporous shell in Pd/SiO_2@Ti-MS, SiO_2@Pd(R)/Ti-MS, and SiO_2@Pd(S)/Ti-MS, respectively. The average size of the Pd NPs was 3.1 – 3.2 nm, and no significant difference in the Pd NP size was observed in the three samples.

The textural properties, characterized by N_2 adsorption–desorption measurements, TEM, and inductively coupled plasma spectroscopy (ICP), are summarized in Figure 2.7A. The surface area was significantly increased by formation of the Ti-MS shell. The surface area and pore diameter of the SiO_2@Pd(R)/Ti-MS and SiO_2@Pd(S)/Ti-MS catalysts were slightly lower than those of Pd/SiO_2@Ti-MS, which is probably due to covering with Pd NPs. The shell thickness and the Pd and Ti contents were almost constant for each sample. Ti K-edge X-ray absorption fine structure (XAFS) measurements confirmed that the Ti species in Ti-MS were isolated and of tetrahedral coordination geometry, which is suitable for selective oxidation with H_2O_2 as an oxidizing agent.

The catalytic activities of the samples were first evaluated for the direct synthesis of H_2O_2 from atmospheric H_2 and O_2 gases on the Pd NP sites. The H_2O_2 concentration in the reaction medium after 1 h was comparable for all three catalysts (Figure 2.7B); however, that for SiO_2@Pd(R)/Ti-MS was slightly lower than those for Pd/SiO_2@Ti-MS and SiO_2@Pd(S)/Ti-MS due to disturbance of

reactant diffusion by the random distribution of Pd NPs within the mesopore channels.

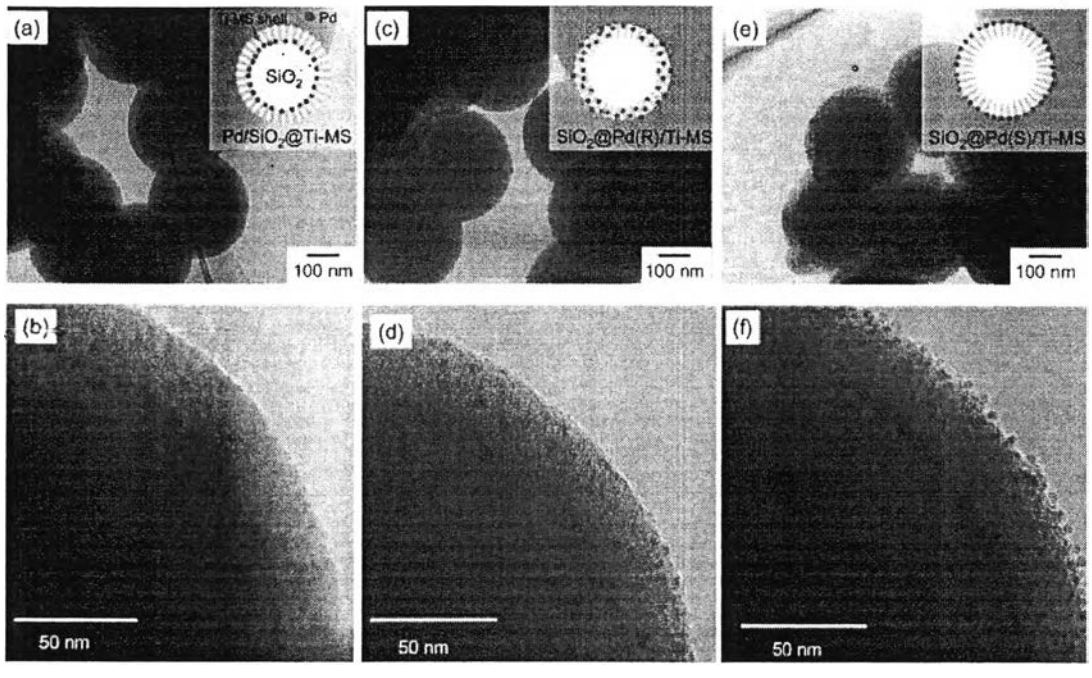

Figure 2.6 HR-TEM images and schematic illustrations (insets) of (a,b) Pd/SiO_2@Ti-MS, (c,d) SiO_2/@Pd(R)/Ti-MS, and (e,f) SiO_2/@Pd(S)/TiMS (Okada *et al.*, 2012).

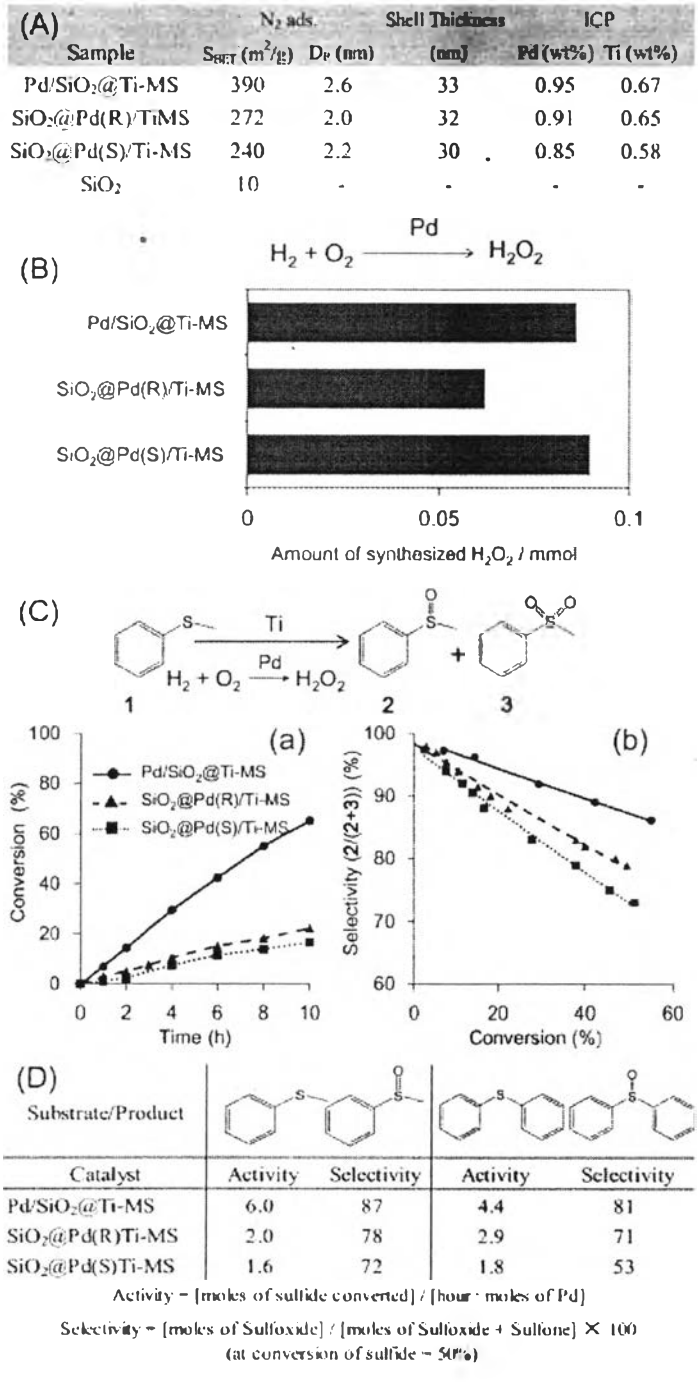

Figure 2.7 (A) Ti-MS shell parameters and metal contents of samples. (B) Amount of H_2O_2 synthesized using Pd/SiO_2@Ti-MS, SiO_2/@Pd(R)/Ti-MS, and SiO_2/@Pd(S)/Ti-MS. (C) (a) Kinetics of methylphenyl sulfide (1) oxidation using in situ generated H_2O_2, and (b) dependence of the conversion level on the selectivity. Selectivity = [2/(2+3)]×100. (D) Catalytic activity and selectivity for sulfoxide in the one-pot oxidation of methyl phenyl sulfide and diphenyl sulfide (Okada *et al.*, 2012).

2.4.2 Effect of Pore Diameter in the Ti-MS Shell

Uniform pore size is one of the unique characteristics of mesoporous silica materials, and it can be easily controlled by changing the SDA employed. It is expected that the mass transport of reactants and products is influenced by the pore size. Therefore, mass transport will become easier, and the reaction rate will be higher, as the pore diameter is increased. Moreover, the shorter residence time of sulfoxide in Ti-MS would contribute to the prevention of over oxidation and sulfone production. Thus, the pore diameter was controlled to clarify the role of the Ti-MS shell.

The simplest method to control the pore diameter is to change the alkyl length of the surfactant as the SDA. The pore diameter of the Pd/SiO_2@Ti-MS type core–shell catalyst was controlled using C_{12}TABr, C_{14}TABr, C_{16}TABr, and C_{18} TACl as the SDAs. Using C_{18}TACl as SDA.

The characterization results of these catalysts are summarized in Figure 2.8. N_2 adsorption–desorption analyses confirmed that the pore diameters were systematically expanded according to the alkyl length of the SDA. Uniform core–shell particles with almost the same shell thickness were formed in each sample, as indicated by TEM analysis. The Brunauer–Emmett–Teller (BET) surface area and pore volume were also increased with the pore diameter.

(A)

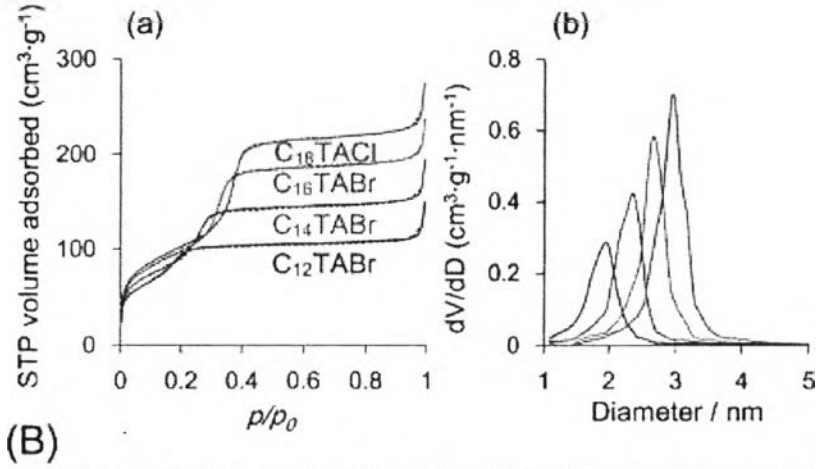

(B)

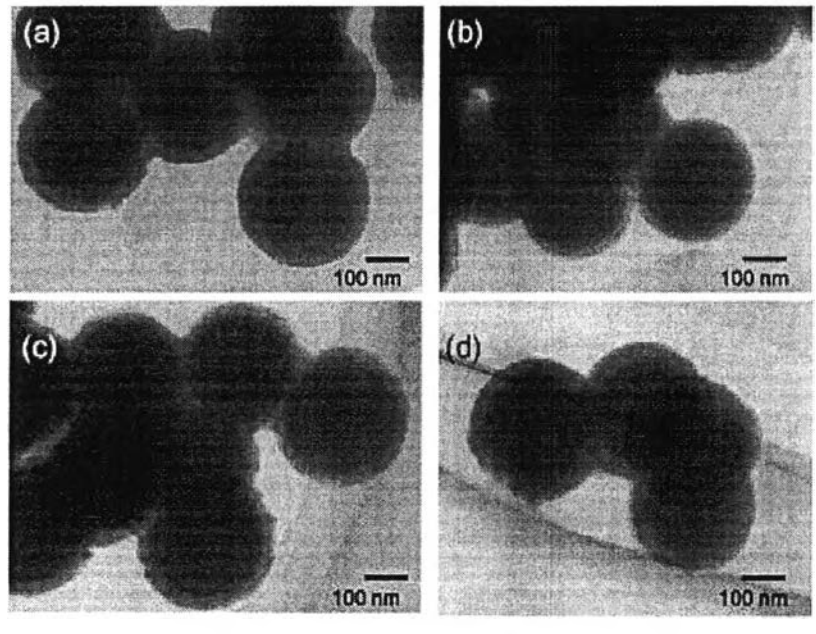

(C)

SDA	S_{BET} (m^2/g)	V_P (cm^3/g)	D_P (nm)
C_{12}TABr	344	0.19	1.9
C_{14}TABr	371	0.27	2.3
C_{16}TABr	390	0.34	2.6
C_{18}TACl	404	0.39	2.9

Figure 2.8 (A) (a) N_2 adsorption–desorption isotherms and (b) BJH pore size distributions. (B) TEM images of Pd/SiO_2@Ti-MS type core–shell catalysts using (a) C_{12}TABr, (b) C_{14}TABr, (c) C_{16}TABr, and (d) C_{18}TACl as template SDAs. (C) Parameters of the Ti-MS shells (Okada *et al.*, 2012).

The results of the one-pot oxidation of using these catalysts are shown in Figures 2.9a and b. The activity and selectivity were improved with an increase in the pore diameter due to enhancement of the diffusion rates of reactants and products within the mesoporous channels. Diffusibility is very important for the catalysis using nanoscale porous materials. The effect of pore diameter in the core–shell catalysts is emphasized by the one-pot oxidation of diphenyl sulfide, which is a bulkier reactant. As illustrated in Figures 2.9c and d, the catalytic activity was improved in the same way. These results confirm the importance of mass transport to achieve high activity and selectivity for a one-pot oxidation reaction.

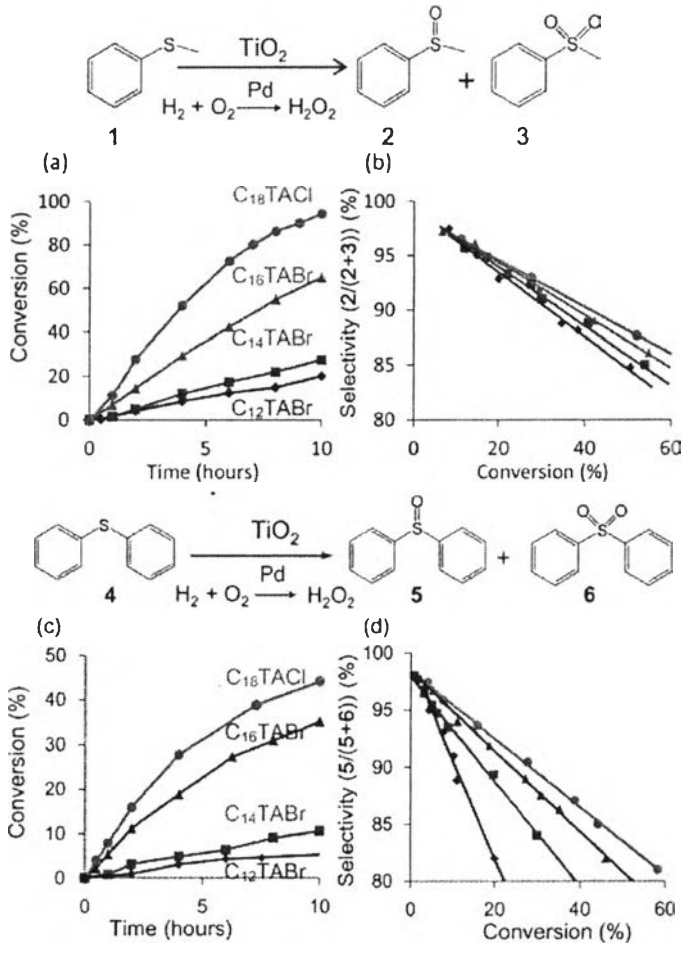

Figure 2.9 (a,c) Kinetics of methyl phenyl sulfide (1) and diphenyl sulfide (4) oxidation using in situ generated H_2O_2, and (b,d) dependence of the conversion level on the selectivity using Pd/SiO_2@Ti-MS type core–shell catalysts with controlled pore diameters (Okada *et al.*, 2012).

2.4.3 Effect of the Ti-MS Shell Thickness

Although it was demonstrated that the core–shell structure influenced the catalytic performance for one-pot oxidation, the role of the TiMS shell remained to be clarified. Therefore, a detailed investigation was performed by varying the shell thickness to elucidate the role of Ti-MS shell for one-pot oxidation. It is anticipated that an extremely thin Ti-MS shell would not allow efficient utilization of the in situ synthesized H_2O_2 within the mesoporous channels, and that the efficiency would be enhanced by designing an appropriate Ti-MS shell thickness. The thickness of Ti-MS shell can be easily controlled by varying the amount of precursors (TEOS, TPOT) in the presence of C_{18}TACl as the SDA. TEM images of various Pd/SiO_2@Ti-MS type core–shell catalysts prepared using 3, 5, and 7 times the amount of precursors than that used for the original experiment are shown in Figure 2.10. The BET surface area and Barrett–Joyner–Halenda (BJH) pore size determined by N_2 adsorption – desorption analysis, Pd and Ti contents determined by ICP analysis, and the average shell thickness measured by TEM analysis are summarized in Figure 7e. These characteristics can be systematically controlled by varying the amount of precursors, while maintaining mesoporous structures. In the samples of amount of precursor 5× (Figure 2.10c) and 7× (Figure 2.10d), there is some different contrast near the SiO_2 core region. Using 5x amount of precursor shows highest conversion and selectivity as shown in Figure 2.11.

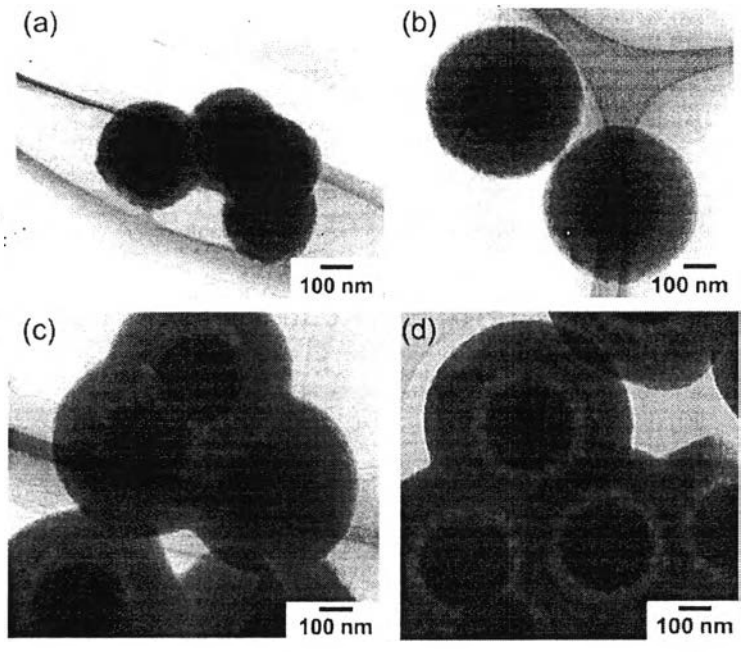

(e)

Amount of Precursor	N_2 ads. S_{BET} (m^2/g)	D_P (nm)	ICP Pd (wt%)	Ti (wt%)	Shell Thickness (nm)
1	404	2.9	0.72	0.50	35
3	641	2.8	0.42	0.94	105
5	769	2.8	0.34	1.15	155
7	930	2.7	0.26	1.30	185

Figure 2.10 TEM images of Pd/SiO_2@Ti-MS type core–shell catalysts with various shell thicknesses, prepared by changing the amount of precursor: (a) 1×, (b) 3×, (c) 5×, and (d) 7×. (e) Ti-MS shell parameters and metal contents of the catalyst samples (Okada *et al.*, 2012).

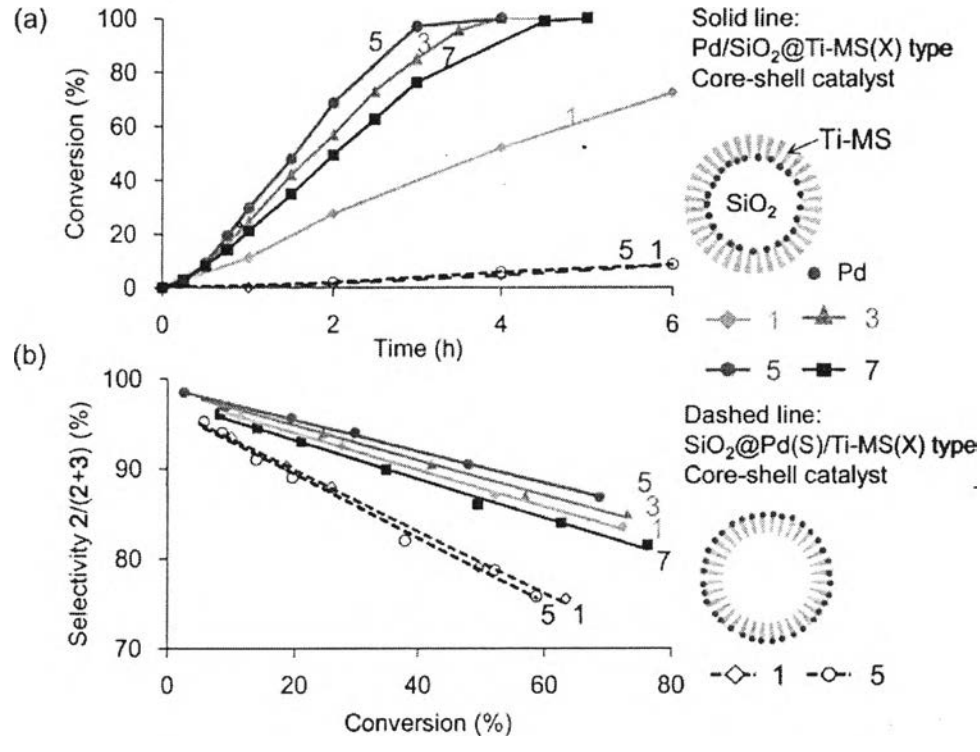

Figure 2.11 (a) Kinetics of methyl phenyl sulfide one-pot oxidation and (b) dependence of the conversion level on the selectivity using Pd/SiO_2@Ti-MS or SiO_2@Pd(S)/Ti-MS type core–shell catalysts with various shell thicknesses (different amounts of precursors; 1, 3, 5, and 7 times the original amount) (Okada *et al.*, 2012).

In conclusion, a new type of core–shell structure catalyst was developed that consisted of Pd NP-supported on a SiO_2 core covered with a Ti-MS shell. The performance of the catalysts fabricated in this study for one-pot oxidation is summarized in Table 2.1. The best core–shell catalyst had approximately 20 times higher activity and better selectivity than a conventional catalyst due to control of the Pd NP position, pore diameter, and thickness of the Ti-MS shell by enhancement of the H_2O_2 utilization efficiency. Therefore, the core–shell catalyst is considered to be a promising structure for one-pot reactions.

Table 2.1 Summary of catalyst sample parameters, activity, and selectivity for one-pot oxidation (Okada *et al.*, 2012)

Sample parameter						Substrate/Product			
Core-shell type	Pd position	SDA	Pore diameter (nm)	Amount of Precursor	Shell Thickness (nm)	Activity	Selectivity	Activity	Selectivity
Pd/SiO$_2$@Ti-MS	Boundry	C_{12}TABr	1.9	1	28	1.8	84	0.6	61
	Boundry	C_{14}TABr	2.3	1	30	2.6	86	1.2	75
	Boundry	C_{16}TABr	2.6	1	33	6.0	87	4.3	80
	Boundry	C_{14}TACl	2.9	1	35	11.2	88	6.3	83
	Boundry	C_{16}TACl	2.8	3	105	28.4	89	27.4	84
	Boundry	C_{16}TACl	2.8	5	155	32.3	90	40.7	87
	Boundry	C_{16}TACl	2.7	7	185	24.8	87	14.9	80
SiO$_2$@Pd/S1Ti-MS	Outer surface	C_{16}TABr	2.1	1	30	1.6	72	1.8	61
	Outer surface	C_{14}TACl	2.2	1	32	1.5	79	1.4	67
	Outer surface	C_{14}TACl	2.5	5	115	1.5	80	1.9	69
SiO$_2$@Pd(R)Ti-MS	Random	C_{16}TABr	2.0	1	30	2.0	78	2.9	71

Activity = [moles of sulfide converted] / [hour · moles of Pd]

Selectivity = [moles of Sulfoxide] / [moles of Sulfoxide + Sulfone] × 100 (at conversion of sulfide = 50%)

Activity = [moles of sulfide converted]/[hour·moles of Pd]. Selectivity = [moles of sulfoxide]/[moles of sulfoxide + sulfone]×100 (at conversion of sulfide = 50%).

Ramya *et al.* (2012) studied liquid hydrocarbon fuels from jatropha oil through catalytic cracking technology using AlMCM-41/ZSM-5 composite catalysts. The hydrothermal syntheses of a microporous solid acid catalyst (HZSM-5 with Si/Al = 14), mesoporous materials (AlMCM-41) with varying Si/Al ratios (Si/Al = 18, 41, 72, and 95) and composite catalyst comprising HZSM-5 (as core) and varying coating percentages (5, 10, and 20 %) of AlMCM-41 (as shell). The catalytic activities of all the synthesized catalysts towards the cracking of jatropha oil obtained at the optimized conditions of temperature 400 °C, WHSV 4.6 h^{-1} and reaction time 1 h. Of all the mesoporous catalysts with varying Si/Al ratios, AlMCM-41 (Si/Al = 18) was found to be the most active catalyst as it converted 65 % of jatropha oil yielding 39% of bioliquid fuel with 47 % and 36 % selectivity towards green diesel and green gasoline respectively. In the core–shell architecture of the composite catalyst, different % coatings of the best active mesoporous material (AlMCM-41, Si/Al = 18) over the best active microporous material (ZSM-5, Si/Al = 14) were done. AlMCM-41(25)/ZSM-5(15) (10 %shell) showed remarkable performance in the conversion of jatropha oil (99 %) yielding 70 % of bio liquid fuel with very high selectivity (61 %) towards green gasoline.

Table 2.2 Conversion and yield of bioliquid fuel in the catalytic conversion of jatropha oil (Ramya *et al.*, 2012)

Catalysts	Conversion (%)	Yield of Bioliquid Fuel (%)
HZSM-5 (Si/Al=14)	62	29
AlMCM-41 (Si/Al=18)	65	39
AlMCM-41 (Si/Al=41)	63	40
AlMCM-41 (Si/Al=72)	60	35
AlMCM-41 (Si/Al=95)	55	32
AlMCM-41/ZSM (5% shell)	94	66
AlMCM-41/ZSM (10% shell)	99	70
AlMCM-41/ZSM (20% shell)	56	28

From Table 2.2 AlMCM-41/ZSM-5 (10 %shell) gave the higher conversion and yield of bio liquid fuel of 99 % and 70 % respectively compare to isolate catalyst. The possible reaction mechanism of vapor phase catalytic cracking of triglyceride molecule over composite catalyst is shown in Figure 2.12. The big shaded circles are mesopore and dark small circles are micropore. Firstly the triglyceride molecules are vaporizing at 400 °C and enter into the mesoporous (shell) layer, it crack into three fractions namely A, B and C as indicated by dotted brackets on the triglyceride. Part 'A' of the triglyceride become propane or propene and part 'B' crack to yield CO and CO_2 in the mesophase. 'C' crack into long chain hydrocarbons length depending on Si/Al ratio of mesophase. These long chain hydrocarbons molecules further enter into the microporous material where the secondary cracking and isomerisation of oil takes place to form bioliquid fuel 'Y'. 'A' gets cracked further into 'X' (C_1–C_3 hydrocarbons), some of them take part in oligomerization and aromatization. Fragment 'B' does not undergo any further reactions.

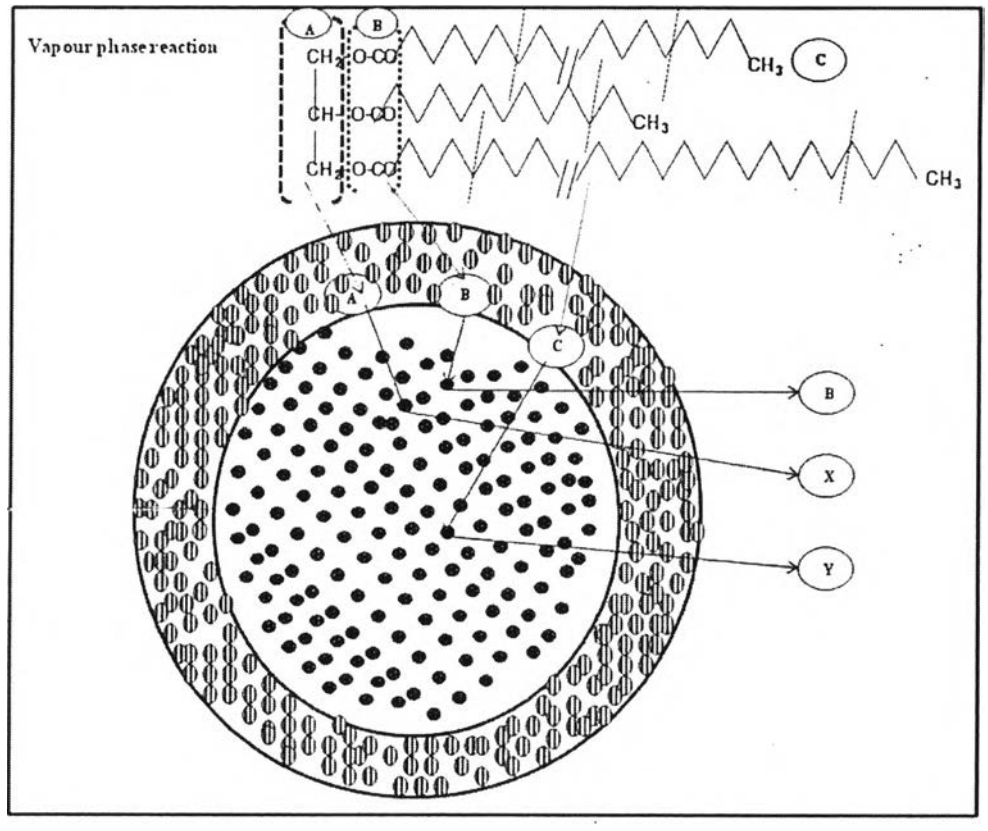

Figure 2.12 Possible cracking mechanism of triglyceride over composite catalyst. A- propane or propene, B- CO or CO_2, C- long chain hydrocarbons, X- C_1–C_3 hydrocarbons, Y –both straight chain and branched hydrocarbons (C_nH_{2n+2}) and aromatics (Ramya *et al.*, 2012).